

In Silico Designing of Thieno[2,3-*b*]thiophene Core-Based Highly Conjugated, Fused-Ring, Near-Infrared Sensitive Non-fullerene Acceptors for Organic Solar Cells

Saleh S. Alarfaji,* Faiz Rasool, Bushra Iqbal, Ajaz Hussain, Riaz Hussain,* Muhammad Akhlaq, and Muhammad Fayyaz ur Rehman



Cite This: *ACS Omega* 2023, 8, 4767–4781



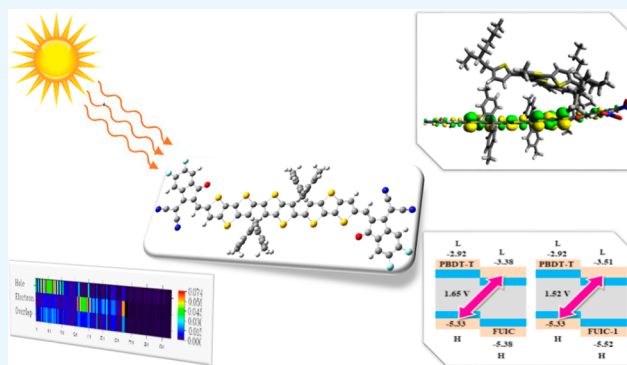
Read Online

ACCESS |

Metrics & More

Article Recommendations

ABSTRACT: The performance of organic solar cells (OSCs) has been improving steadily over the last few years, owing to the optimization of device fabrication, fine-tuning of morphology, and thin-film processing. Thiophene core containing fused ring-type non-fullerene acceptors (NFAs) achieved significant proficiency for highly efficient OSCs. Quantum chemical computations are utilized herein with the motive of suggesting new NIR sensitive, highly efficient low-band gap materials for OSCs. A series of extended conjugated A- π -D- π -A architected novel fused-ring NFAs (FUIC-1-FUIC-6) containing thieno[2,3-*b*]thiophene-based donor core are proposed by substituting the end-capped units of synthesized molecule F10IC. Different properties including frontier molecular orbital analysis, density of states analysis, transition density matrix analysis, excitation energy, reorganizational energies of both holes (λ_h) and electrons (λ_e), and open-circuit voltage (V_{oc}) were performed employing the density functional theory approach. Charge transfer analysis of the best-designed molecule with the donor complex was analyzed to comprehend the efficiency of novel constructed molecules (FUIC-1–FUIC-6) and compared with the reference. End-capped acceptor alteration induces the reduction of the energy gap between HOMO–LUMO (1.88 eV), tunes the energy levels, longer absorption in the visible and near-infrared regions, larger V_{oc} , smaller reorganizational energies, and binding energy values in designed structures (FUIC-1–FUIC-6) in comparison to reference (FUIC). The designed molecules show the best agreement with the PTBT-T donor polymer blend and cause the highest charge from the HOMO to the LUMO orbital. Our findings predicted that thieno[2,3-*b*] thiophene-based newly designed molecules would be efficient NFAs with outstanding photovoltaic characteristics and can be used in future applications of OSCs.



1. INTRODUCTION

Energy is essential for financial progression and human survival, but its resources are decreasing daily.¹ The most acceptable source of renewable energy is solar cells since they are clean, non-polluting, have a low cost, are distributed worldwide, and are non-exhaustive.² A solar cell is a device that converts sunlight directly into electrical energy via the photovoltaic effect.^{3–5} Organic solar cells, also known as OSCs, have become fascinating because of their benefits of being inexpensive, having a vast selection of organic materials, being solution processable, and having the potential to be used in large-area devices.^{6–8} To increase the OSC power conversion efficiencies (PCEs), light-absorbing materials have been widely studied.⁹ In fact, the device physics also plays a vital role in improving the performance of OSCs.^{10–13} As an alternative to fullerenes in organic photovoltaics, non-fullerene acceptors (NFAs) enable the rapid progress of OSCs with higher PCEs.^{14–16} Recently reported fused-ring acceptor–

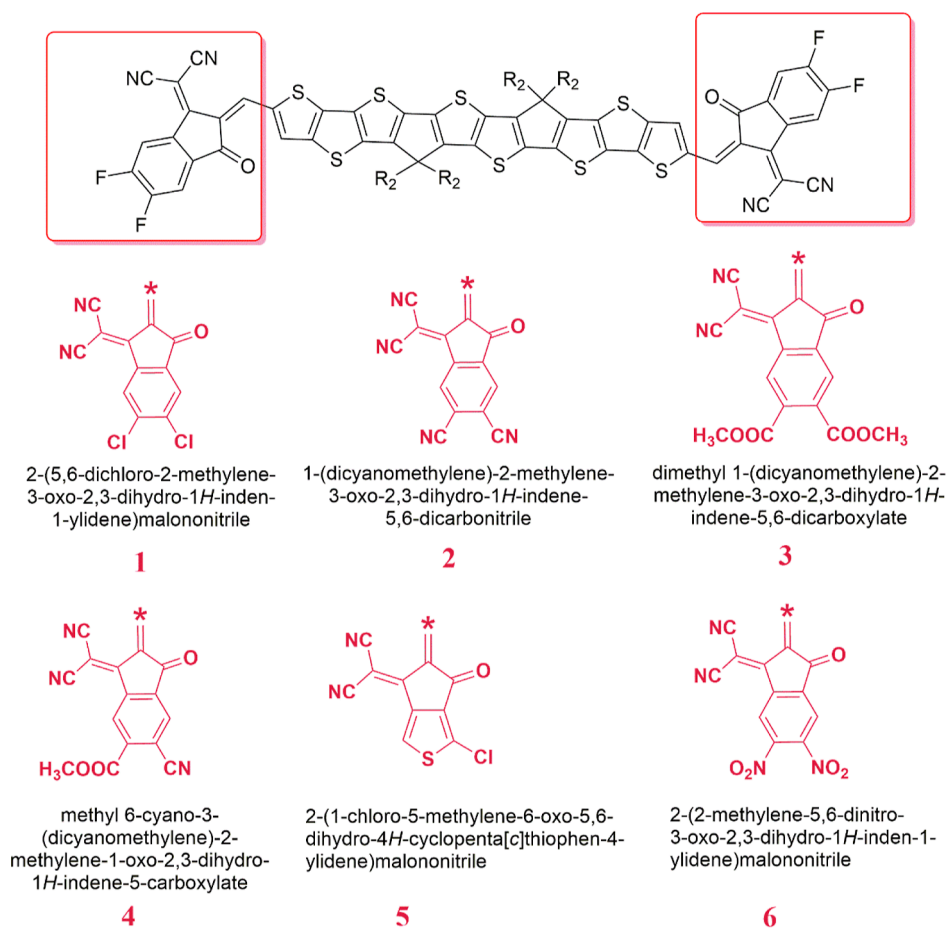
donor–acceptor (A–D–A)-type organic compounds containing effective two-photon absorption have resulted in a significant increase in photovoltaic competence OSCs.^{17–19} Since they are electronically coupled in-plane to acceptor groups at the molecule's edge, electron-rich cores, planar, stiff, and highly delocalized π -systems, these materials' structural motifs are also intriguing for two-photon absorption (2PA).^{20,21} Examples with strong, long wavelength 1PA are likely candidates for strong 2PA that extend into the near-infrared (NIR). The extensive material design efforts that were

Received: October 25, 2022

Accepted: January 17, 2023

Published: January 27, 2023



Scheme 1. Schematic Diagram Representing Different End-Capped Acceptors (1–6) for Designing Thieno[2,3-*b*]thiophene-Based NFAs

made to maximize the competency and spectrum range of a 2PA material are substantially responsible for the success of these endeavors. The many synthetic chemistries that can be used to modify the structures of conjugated molecules and polymers to produce strong 2PA responses is one of the many benefits of organic materials.^{22,23}

Due to the significant 2PA increases that can be obtained through careful adjustments in their structural makeup, highly delocalized π -systems containing quadrupolar molecules, particularly, have attracted much attention. For their two-photon absorption (2PA) capabilities in organic photovoltaics, Allen et al. created quadrupolar A–D–A architecture based on fused-ring-type organic chromophores (F10IC).²⁴ The F10IC has thieno[3,2-*b*]thiophene at its core as a donor, and indacene (IND)-centered analogues serve as the electron acceptors in the F10IC. In the scientific literature, modifications to the size, planarity, functionalization, and geometry of compounds containing π -conjugated fused rings have been shown to substantially influence the compounds' optoelectronic competencies.^{20,21} The addition of spacers among terminal moieties, conjugated rings of donors, and additional electron-withdrawing and conjugated acceptors can improve the photovoltaic characteristics of molecular frameworks.^{25,26} The amount of quadrupolar ground-to-excited-state charge transfer (CT) is also controllable by adjusting the strength of the acceptor (A). Using electron-deficient and rich structural motifs for building OSCs is one of the molecular engineering techniques for designing non-fullerene acceptors (NFAs).

Through the flexible structural adjustability, such a combination of electron-donating and electron-withdrawing moiety could create an electron donor–acceptor (D–A) architecture that is advantageous for adjusting the frontier orbital levels, band gap, light-absorption capacity, intramolecular CT, and intermolecular charge separation and recombination.^{27–29}

Under these assumptions, it is intended to change the IND-centered analogues of the F10IC with strong reported end-capped acceptors with efficient electron-withdrawing features for developing innovative non-fullerene acceptors while maintaining the donor core of the thieno[3,2-*b*]thiophene. Researchers are increasingly using density functional theory (DFT) and time-dependent density functional theory (TDDFT) approaches to explore the photoelectric characteristics of organic semiconductors and identify potential candidates for solar cell applications. First-principles computational molecular design could provide an effective method to forecast the qualities we are interested in, avoiding the need for experimental trial-and-error searches for new materials. In this work, we aim to inaugurate structure–property connections of thieno[3,2-*b*]thiophene-based molecules to evaluate the optoelectronic viability of these cutting-edge materials and conduct a computational investigation on the effect of the enhanced electron-pulling capacity of the terminal IND on their photovoltaic performance. We calculated various parameters, including the frontier molecular orbital (FMO), the density of state (DOS) transition density matrix (TDM), absorption maxima, reorganizational energies, excitation

energy, and open-circuit voltage. Charge-transfer analysis was also carried out on the optimally designed molecules in conjunction with the suitable donor complexes, and the results were compared to those of the reference molecule (FUIC). We are optimistic that these freshly developed chemicals will make promising high-performance OSC candidates.

2. RESULTS AND DISCUSSION

The focus of this study is to construct and investigate novel A- π -D- π -A quadrupolar-type fused-ring, highly conjugated acceptors with improved optoelectronic assets for their usage in solar cells. For this, F10IC,²⁴ which is a novel fused-ring, highly conjugated, A- π -D- π -A backbone having thieno[2,3-*b*] thiophene-based core as the donor moiety and 2-(5,6-difluoro-2-methylene-3-oxo-2,3-dihydro-1*H*-inden-1-ylidene)-malononitrile as end-capped acceptor groups with significant electron-withdrawing properties,²⁴ is used as a reference molecule (F10IC) in this report. In structural tailoring of the reference F10IC, the acceptor unit of F10IC is switched using six dissimilar designed end-capped acceptors (1–6), as represented in Scheme 1, and six novel A- π -D- π -A acceptor molecules (FUIC-1–FUIC-6) are being proposed for promising photovoltaic and optoelectronic applications. The central donor core was kept fixed while end-capped units were changed to design the similar core-based efficient new molecules. The names of the end-capped acceptors (1–6) are mentioned in Scheme 1.

Long alkyl chains in the reference and developed compounds (FUIC and FUIC-1–FUIC-6) were swapped with methyl groups to save computational expenses. According to earlier publications, these simplifications do not affect the relative features of the acquired values or the essential features of the studied molecules.³⁰ Numerous functionals are examined in this quantum chemistry inquiry to determine the best functional for estimating the photovoltaic and optoelectronic characteristics of designed structures.

Figure 1 depicts a bar chart comparing experimental λ_{\max} values of the reference (FUIC) molecule to DFT-estimated values in chloroform at different functionals. The calculated values of λ_{\max} at B3LYP, CAM-B3LYP, B3PW91, MPW1PW91, and ω B97XD/6-31G(d,p) functionals are 845, 580, 595, 780, and 601 nm correspondingly. The maximum

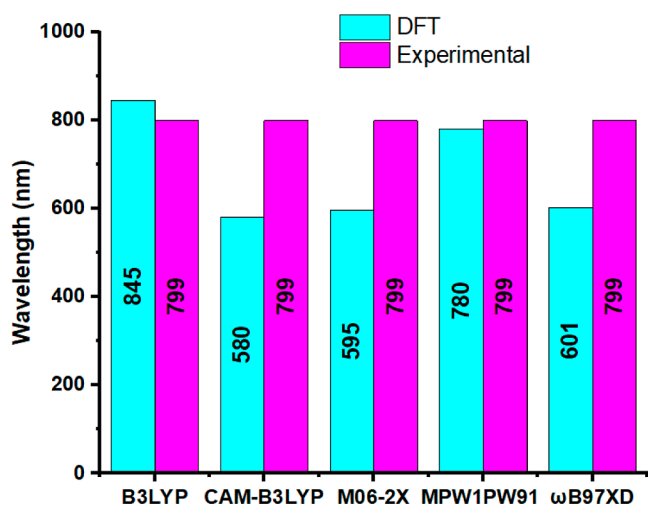


Figure 1. Bar chart representation for selection of DFT functional.

wavelength measured experimentally for the standard molecule is 799 nm.²⁴ Therefore, MPW1PW91/6-31G (d,p) functional demonstrates the most satisfactory compatibility with the reported highest absorption, and it can be employed for further analysis of FUIC and designed (FUIC-1–FUIC-9) molecule.

The optimized structures of all the designed molecules at the MPW1PW91/6-31G(d,p) functional are displayed in Figure 2.

2.1. Frontier Molecular Orbital (FMO) Analysis. FMO is critical in understanding charge conduction and conducting electricity. The sequence of HOMO and LUMO is considered necessary in OSCs to transfer charge.^{31,32} In OSCs, the conduction band can be regarded as HOMO, and the valence band is considered LUMO according to the Band theory. Meanwhile, the difference between the conduction and valence bands is called a band gap.^{33,34} The photovoltaic character has considerable dependence on the band gap value. The band gap value is not only crucial for the FMOs but is also employed for the determination of V_{oc} and binding energy (E_b). The good efficiency of OSCs is related to the lower band gap value and vice versa.³⁵ With the help of FMO analysis, we can predict the conduction behavior of FUIC and FUIC-1 to FUIC-6. The HOMO and LUMO energies, together with the band gaps for FUIC and FUIC-1–FUIC-6, are displayed in electron Volts in Table 1.

Table 1 represents the HOMO (−5.38 eV) and LUMO (−3.38 eV) for reference FUIC, and the energy gap is 1.99 eV. For designed molecules, we used different end-capped to enhance the efficiency by decreasing the energy gap. The HOMO energy values in electron Volts are calculated as −5.52, −5.79, −5.48, −5.60, −5.46, and 5.81 eV for FUIC-1, FUIC-2, FUIC-3, FUIC-4, FUIC-5, and FUIC-6, respectively. On the other hand, LUMO energy values calculated for FUIC-1, FUIC-2, FUIC-3, FUIC-4, FUIC-5, and FUIC-6 are −3.51, −3.89, −3.47, −3.64, −3.45, and −3.93 eV, respectively.

From the HOMO and LUMO values, the band gap was predicted as 2.01, 1.90, 2.01, 1.96, 2.01, and 1.88 eV for FUIC-1, FUIC-2, FUIC-3, FUIC-4, FUIC-5, and FUIC-6, respectively. The lowest energy gap is observed for FUIC-6 (1.88 eV). This is because of two efficient electron-withdrawing groups (CN and NO₂) in this structure that extended the conjugation. Overall, CN, COOCH₃, and NO₂ containing units in end-capped acceptors 2, 4, and 6 lowered the energy gap than the reference. From the data, it can be predicted that the descending sequence of the HOMO and LUMO band gap of the designed structures (FUIC-1 to FUIC-6) and reference molecule (FUIC) is FUIC-1 = FUIC-3 = FUIC-5 > FUIC > FUIC-4 > FUIC-2 > FUIC-6. It is concluded that among all, the FUIC-6 molecule has the lowest band gap value. Lower energy gap values imply an efficient design of molecules and their propensity to transform more considerable charges, eventually aiding in the expansion of photovoltaic features. To have further insights into charge delocalization and shifting of density in different parts of investigated molecules, HOMO LUMO diagrams are generated and portrayed in Figure 3.

The green color indicates the positive sites, while yellow pointing to the negative ends. The repetitive pattern of FUIC and FUIC-1 to FUIC-6 demonstrates the right strategy to architect the molecules. Charge resides on the donor core in HOMO and on the acceptors in case of LUMO. This promotes efficient CT. Through prolonged conjugation bridges, the charge was transferred from the donor HOMO to the LUMO end cap, creating a charge separation state that

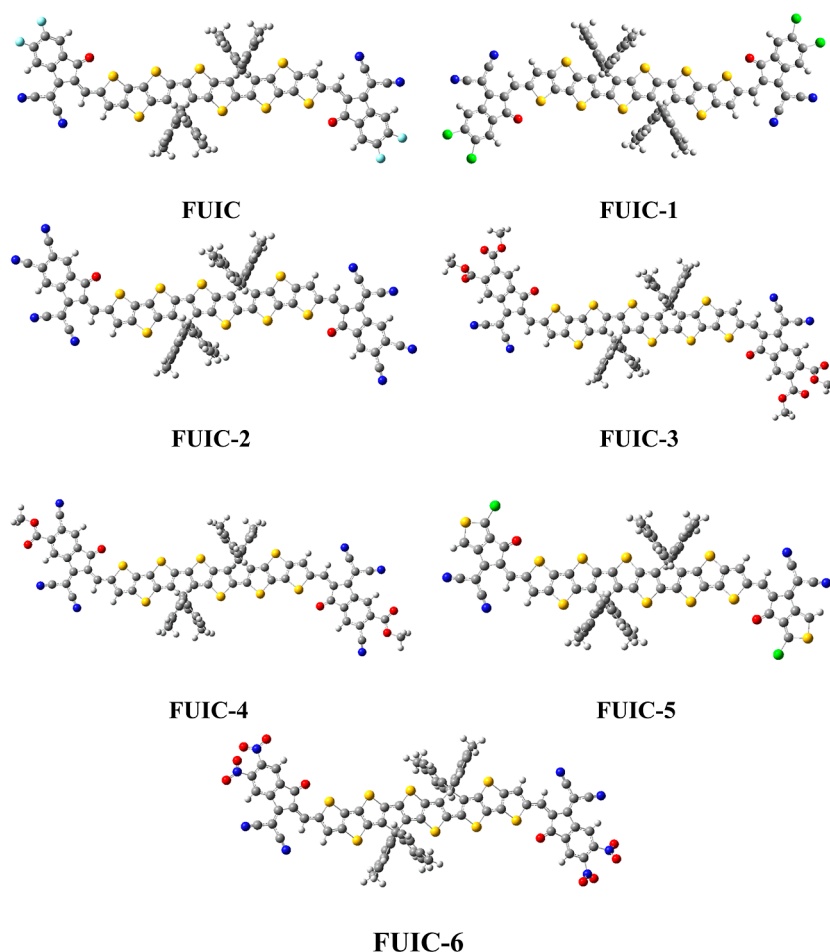


Figure 2. Optimized structure of FUIIC and constructed (FUIIC-1–FUIIC-6).

Table 1. FMOs and Their Energy Gap Values of FUIIC and FUIIC-1 to FUIIC-6

molecules	E_{HOMO}	E_{LUMO}	$E_{\text{gap}} = E_{\text{LUMO}} - E_{\text{HOMO}}$
FUIIC	−5.38	−3.38	1.99
FUIIC-1	−5.52	−3.51	2.01
FUIIC-2	−5.79	−3.89	1.90
FUIIC-3	−5.48	−3.47	2.01
FUIIC-4	−5.60	−3.64	1.96
FUIIC-5	−5.46	−3.45	2.01
FUIIC-6	−5.81	−3.93	1.88

should improve the photocatalytic activity of these newly created near-infrared sensitive NFAs.

2.2. Density of States and Optical Density of States.

The density of states (DOS) and optical density of states (ODOS) analyses are also carried out to strengthen the FMO at DFT/MP1PW91/6-31G(d,p). It can forecast the percentage contribution value for all the fragments present in the molecule.^{36,37} It also gives important information about charge distribution.³⁸ Figure 4 represents the percentage impact of the donor and acceptor sections in each molecule. Regarding FUIIC, 84.7% of the contribution was from donors and 15.3% from acceptors in the case of HOMO. In contrast, the trend was reversed in the case of LUMO, that is, 43.1% of donors and 56.9% of acceptors. Then, the improved trend was observed in designed molecules. For donors, the percentage contribution values of HOMO are 80.3, 83.2, 84.3, 84.3, 83.8,

and 83.2 for FUIIC-1, FUIIC-2, FUIIC-3, FUIIC-4, FUIIC-5, and FUIIC-6, respectively. Consequently, for acceptors, percentage contribution of HOMO is 19.7, 16.8, 15.7, and 16.8%, for FUIIC-1, FUIIC-2, FUIIC-3, FUIIC-4, FUIIC-5, and FUIIC-6, respectively. In donors, the percentage contribution values of LUMO are 33.1, 37.0, 39.8, 38.4, 43.8, and 34% for FUIIC-1, FUIIC-2, FUIIC-3, FUIIC-4, FUIIC-5, and FUIIC-6, respectively.

Ultimately, in acceptors, these values are 66.9, 63.0, 60.2, 61.6, 56.2, and 66.0%, for FUIIC-1, FUIIC-2, FUIIC-3, FUIIC-4, FUIIC-5, and FUIIC-6 correspondingly. All evidence points to the terminal acceptor part of designed compounds being more densely inhabited by LUMO states than the central core HOMO states. For an intramolecular CT to occur, there must be a movement of charge density from the donor via the bridge and finally to the end-capped acceptors. This demonstrates the efficacy of our end-capped modification technique in creating novel NFAs with desirable photovoltaic properties for OSCs.

2.3. Optical Properties.

TDDFT calculations were employed to determine the optical features of the investigated molecules (FUIIC and FUIIC-1–FUIIC-6) using UV–visible analysis in chloroform and gas.^{39,40} For the determination of the photophysical properties of FUIIC and FUIIC-1–FUIIC-6, the conductor-like polarizable continuum model (CPCM) model is applied in chloroform. Tables 2 and 3 summarize the findings of E , f_{os} , λ_{max} , and transition natures in studied molecules (FUIIC and FUIIC-1–FUIIC-6) measured in solvent and gas phases.

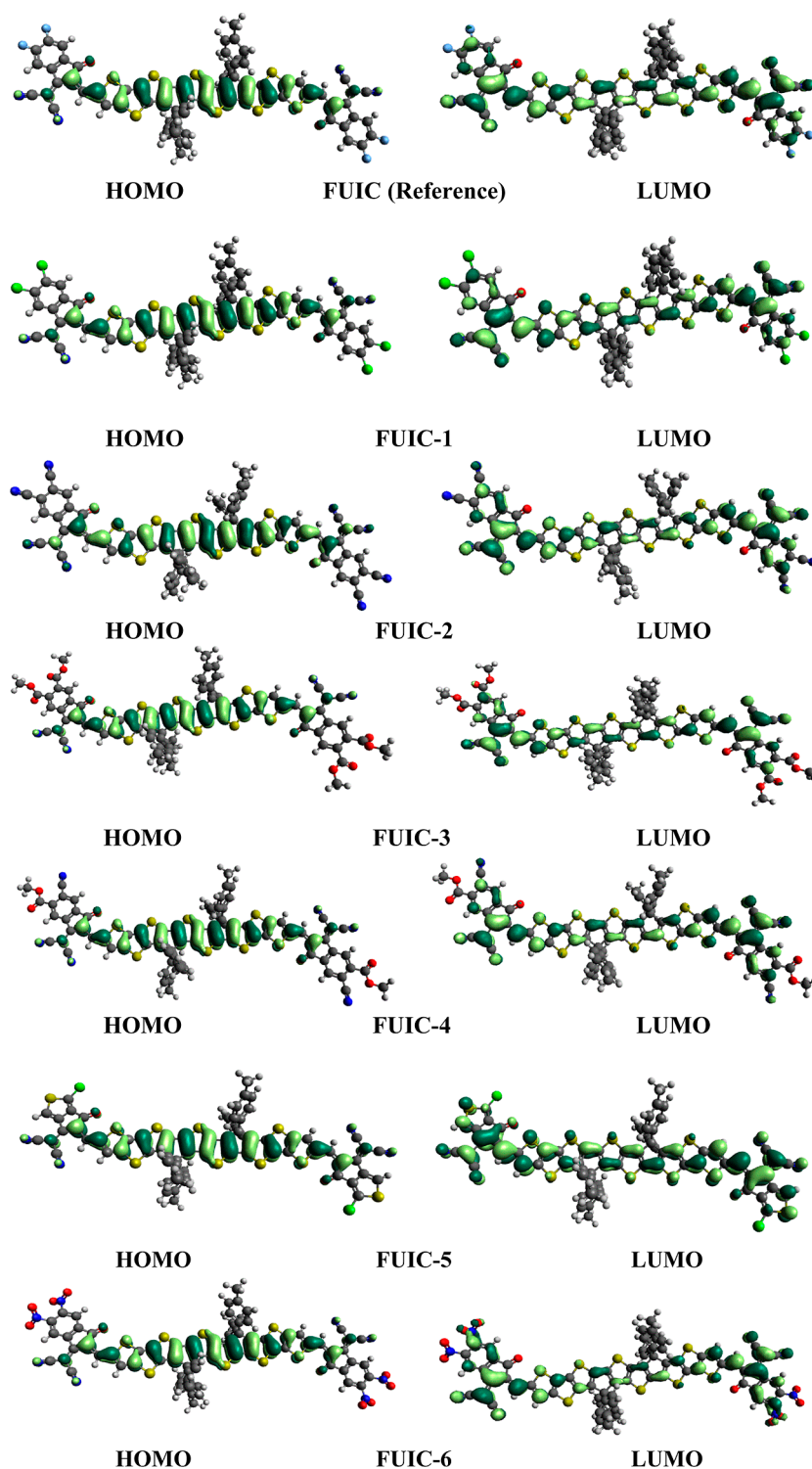


Figure 3. FMOs diagrams of FUIC and constructed molecules FUIC-1–FUIC-6.

The λ_{\max} of the FUIC is obtained at 780.01 nm, which is in good accordance with the experimentally recorded λ_{\max} of 799 nm²⁴ for solvent, as illustrated in Table 2. The λ_{\max} values of the entire investigated systems (FUIC and FUIC-1–FUIC-6) are revealed in Tables 2 (for solvent) and 3 (for gas). In the solvent phase, the order of λ_{\max} values is FUIC-6 > FUIC-2 > FUIC-4 > FUIC-3 > FUIC-1 > FUIC-5 > FUIC while in the gas phase, it is FUIC-6 > FUIC-2 > FUIC-4 > FUIC-3 > FUIC-1 > FUIC-5 > FUIC. The λ_{\max} values of all six designed

molecules FUIC-1–FUIC-6 are greater than the FUIC molecule. In both solvent and gas phases, the proposed FUIC-5 molecule has the smallest, and the FUIC-6 structure has the largest λ_{\max} among all the designed molecules FUIC-1–FUIC-6. End-capped acceptors affect the λ_{\max} values of all investigated molecules because of electron-withdrawing groups present in the end-capped units. The λ_{\max} of FUIC-1 is 780.01 nm (in the solvent) and 729.87 nm in the gas phase, which are slightly greater than the FUIC molecule due to the occurrence

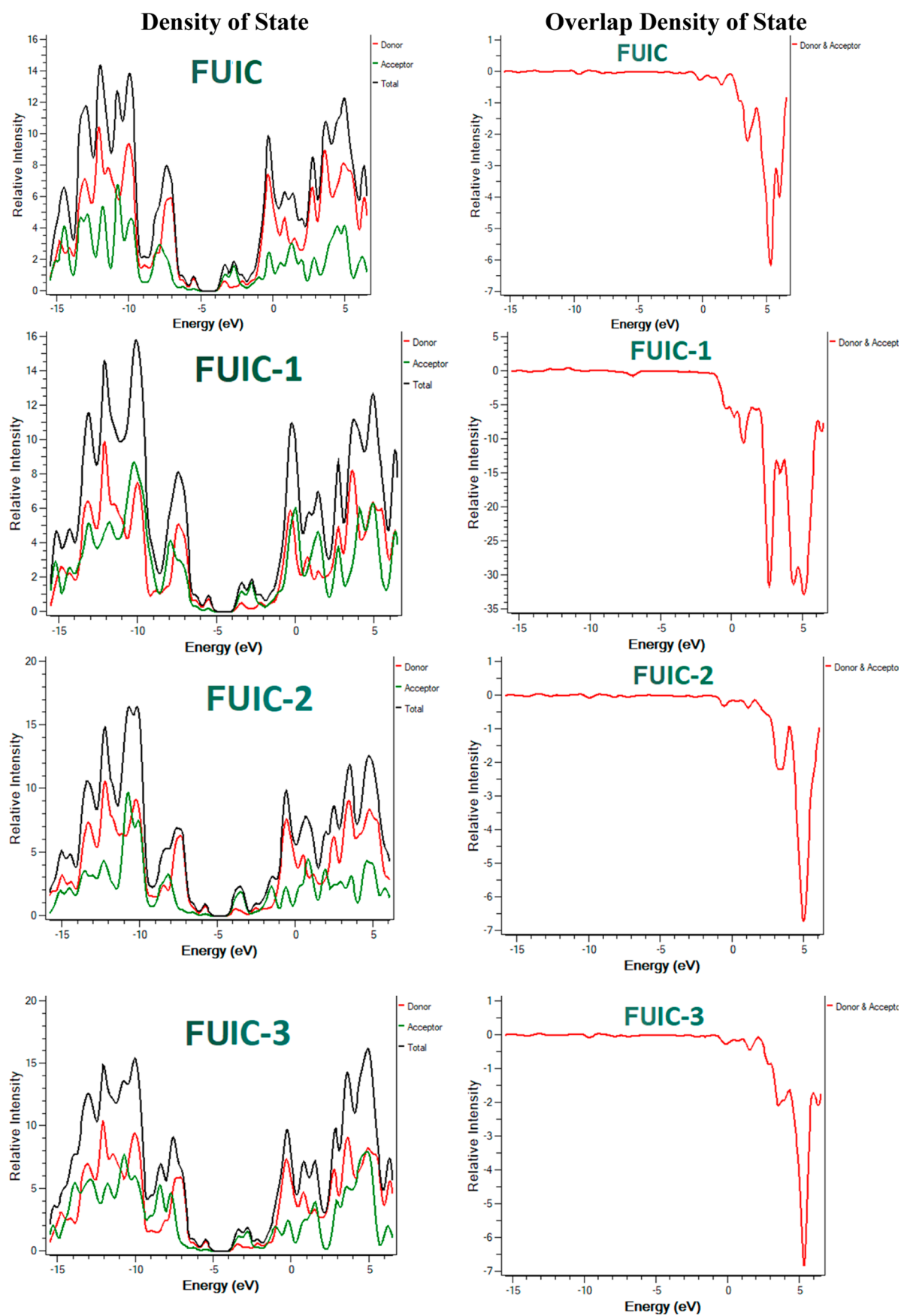


Figure 4. continued

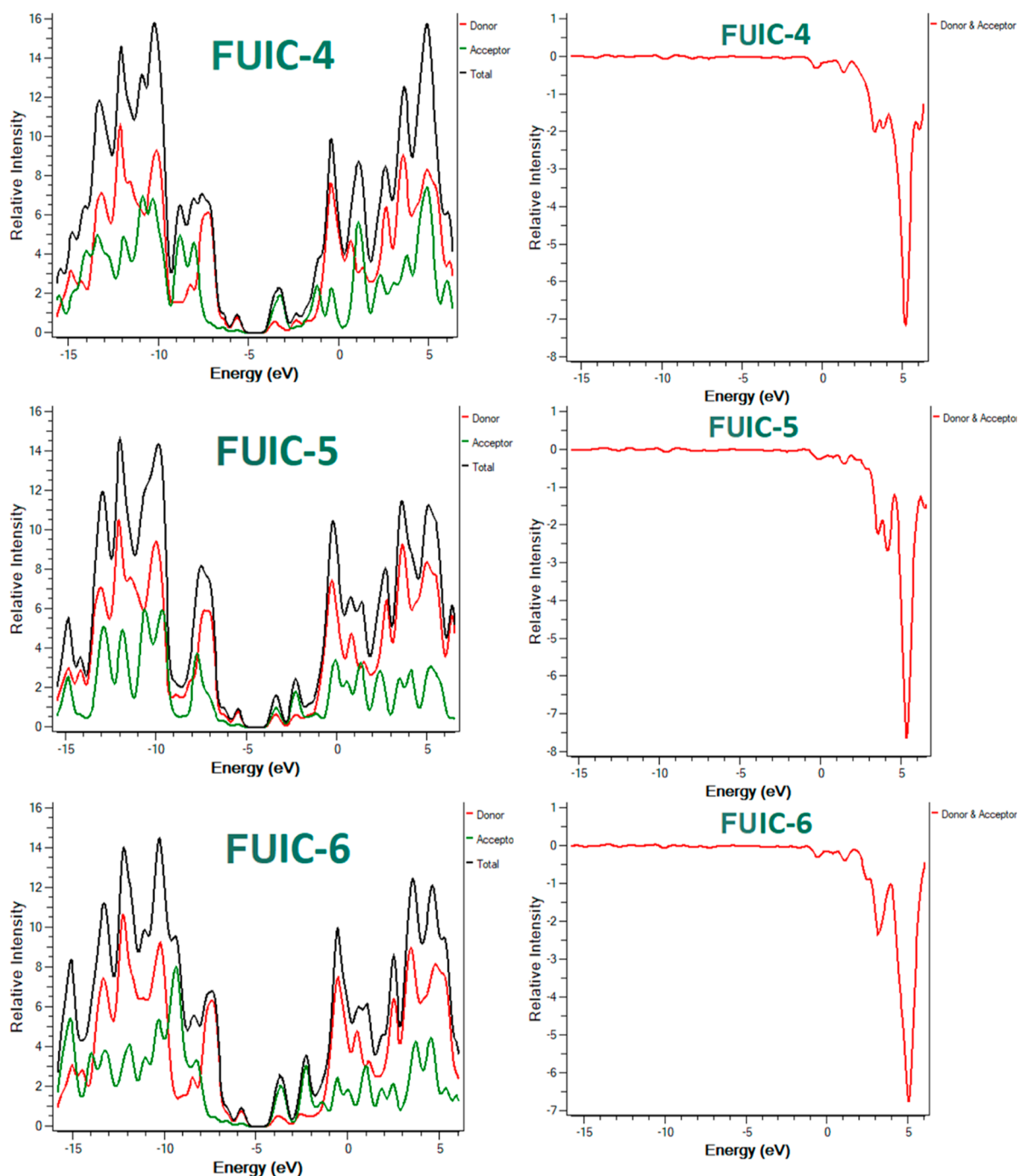


Figure 4. DOS and ODOS around the HOMO LUMO for FUIC and FUIC-1–FUIC-6 graphs.

of chloro (Cl) on end-capped acceptors. The end-capped 2 in FUIC-2, having two cyano (CN) groups on both ends of the molecule, has a stronger withdrawing effect and shifts the absorption maximum toward a longer wavelength (846.12 nm in the solvent and 770.08 nm in the gas phase). The acceptor 3 contains two ester groups (COOCH_3) in the FUIC-3 molecule that cause higher absorption values of 803.26 nm (in the solvent) and 732.41 nm (in the gas phase) than to FUIC, FUIC-1, and FUIC-5. The combined effect of (COOCH_3) and (CN) groups on end-capped acceptor 4 are smaller than end-capped acceptor 3. FUIC-5 molecule shows λ_{max} values of 788.79 nm in the solvent and 728.24 nm in the gas phase, which is smaller than all other designed molecules because of

the lower effect of five terminal acceptors (end-capped). The λ_{max} values of the FUIC-6 designed molecule are 862.31 nm in the solvent and 776.98 nm in the gas phase, which are the highest among all other reference and designed molecules. The reason is that the end-capped acceptors contain two nitro (NO_2) groups with the highest pulling effect and extended conjugation in contrast to all other groups. The ascending order of end-capped acceptors' capability is $6 > 2 > 4 > 3 > 1 > 5$, which is identical to their performance in reducing energy band gaps. Moreover, the decreasing sequence of λ_{max} values shows better accordance with the rising sequence of the energy gap, which is applicable for designing and developing high-

Table 2. Calculated E (Transition Energy), f_{os} (Oscillator Strengths), λ_{max} (Maximum Absorption Wavelengths), and Transition Natures of FUIC and FUIC-1–FUIC-6 in eV at DFT/MPW1PW91/6-31G(d,p) Functional in Chloroform (Solvent)

molecules	calculated λ_{max} (nm)	expected λ_{max} (nm)	E_x (eV)	f_{os}	major MO assignments ^a
FUIC	780.01	799 ²⁴	1.59	3.48	H → L (97%)
FUIC-1	792.98		1.56	3.56	H → L (96%)
FUIC-2	846.12		1.46	3.31	H → L (96%)
FUIC-3	803.26		1.54	3.42	H → L (96%)
FUIC-4	817.72		1.51	3.38	H → L (96%)
FUIC-5	788.79		1.57	3.62	H → L (97%)
FUIC-6	862.31		1.43	2.88	H → L (96%)

^aH = HOMO; L = LUMO.

Table 3. Calculated E (Transition Energy), f_{os} (Oscillator Strengths), λ_{max} (Maximum Absorption Wavelengths), and Transition Natures of FUIC and FUIC-1–FUIC-6 in eV at DFT/MPW1PW91/6-31G(d,p) Functional in the Gas Phase

molecules	calculated λ_{max} (nm)	expected λ_{max} (nm)	E_x (eV)	f_{os}	major MO assignments ^a
FUIC	717.71		1.72	3.16	H → L (98%)
FUIC-1	729.87		1.69	3.26	H → L (98%)
FUIC-2	770.08		1.61	3.09	H → L (98%)
FUIC-3	732.41		1.69	3.18	H → L (98%)
FUIC-4	746.66		1.66	3.19	H → L (98%)
FUIC-5	728.24		1.71	3.25	H → L (98%)
FUIC-6	776.98		1.59	2.83	H → L (98%)

^aH = HOMO; L = LUMO.

performance NFAs molecules with improved optoelectronic properties.

The UV spectra of FUIC and FUIC-1–FUIC-6 computed in both gas and solvent phases are illustrated in Figure 5a,b, which show that end-capped acceptors had a remarkable impact on the values of λ_{max} by promoting the absorption in near IR spectra with lower excitation energy and same significant MO contribution in all of the investigated molecules. Alteration of end-capped (acceptor moieties) is a powerful technique to fine-tune the optoelectronic character-

istics by reducing the transition energy and increasing the absorption values, as shown in the previous discussion. As a result, novel created molecules offer greater optoelectronic capabilities than FUIC, which would increase their demand for solar energy.

Another parameter that improved the optoelectronic features of SCs is the excitation E . Compared to the reference (1.72 eV), all of our created molecules have smaller excitation energy values (1.59–1.71 eV) that are generally thought to be more favorable for efficient photovoltaic properties. Additionally, more outstanding CTs occur from lesser excitation energy, and reduced excitation energy results in the maximum power conversion efficiencies. The descending sequence of excitation energy for all examined structures is FUIC-6 < FUIC-2 < FUIC-4 < FUIC-3 = FUIC-1 < FUIC-5 < FUIC in both solvent and gas phases. This seems applicable for designing molecules that are good candidates for obtaining excellent optoelectronic features.

2.4. Reorganizational Energy. Another valuable tool used to measure the overall CT between donor and acceptor components is reorganizational energy.⁴¹ In most cases, two distinct forms of reorganizational energy exist. The first refers to the reorganizational energy (λ_{int}) generated within a system, while the second refers to the reorganizational energy (λ_{ext}) generated outside a system. The λ_{int} explains variation in the internal structure, and λ_{ext} gives information about variations in the external environment.^{42,43} Marcus' equation calculates reorganization energy. The hole λ_h and electron λ_e reorganizational energy values of FUIC and FUIC-1–FUIC6 are computed at MPW1PW91/6-31G(d,p) functional, and findings are mentioned in Table 4.

Table 4. Reorganizational Energy Values of the Hole and Electron for FUIC and FUIC1–FUIC6

molecules	λ_e (E_h)	λ_h (E_h)
FUIC	0.0053	0.0082
FUIC-1	0.0049	0.0082
FUIC-2	0.0035	0.0079
FUIC-3	0.0050	0.0083
FUIC-4	0.0043	0.0081
FUIC-5	0.0050	0.0080
FUIC-6	0.0043	0.0081

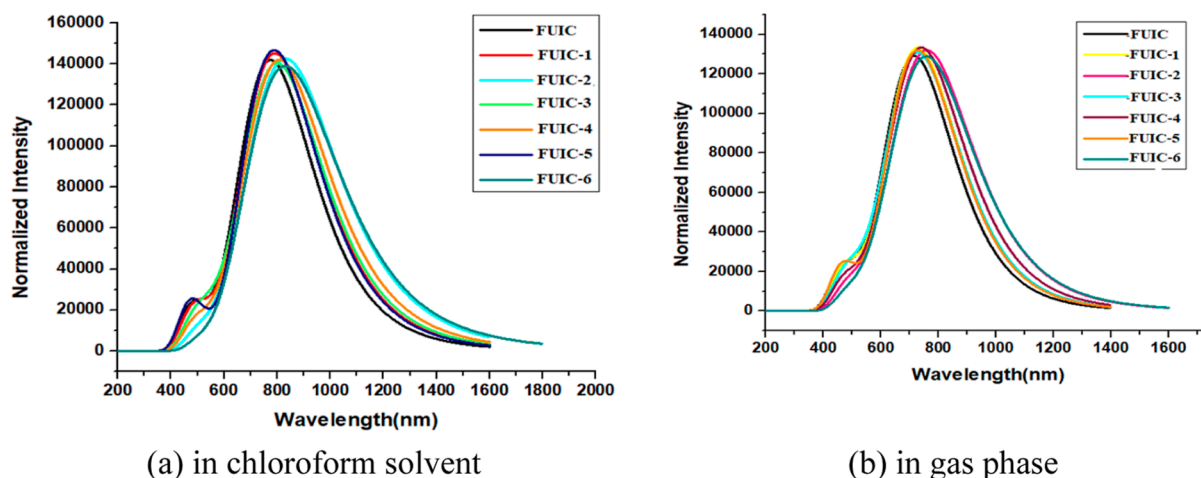


Figure 5. UV–visible absorption spectra (a) in the chloroform solvent and (b) in the gas phase.

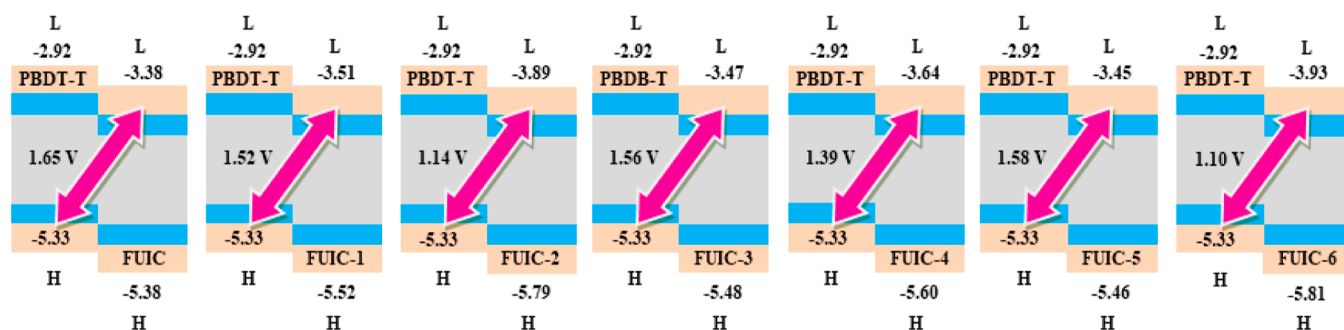


Figure 6. V_{oc} of FUIIC and designed structures FUIIC-1–FUIIC-6.

It is clear from Table 4 that λ_e and λ_h statics reveal remarkable findings. The value of λ_e for FUIIC is computed as 0.0053 eV, and λ_e value of designed molecules (FUIIC-1–FUIIC-6) is calculated as 0.0049, 0.0034, 0.0049, 0.0042, 0.0049, and 0.0043 eV correspondingly. The increasing order for λ_e values of reference FUIIC and designed compounds (FUIIC-1–FUIIC-6) is FUIIC-2 < FUIIC-4 < FUIIC-6 < FUIIC-1 < FUIIC-5 < FUIIC-3 < FUIIC. The calculated λ_e values for all the engineered molecules are lower than those of the reference FUIIC. The λ_h value of FUIIC is calculated as 0.0082. In contrast, λ_h value of constructed molecules is computed as 0.0081, 0.0079, 0.0083, 0.0081, 0.0080, and 0.0080 eV, respectively. The increasing order for λ_h is FUIIC-2 < FUIIC-5 < FUIIC-6 < FUIIC-4 < FUIIC-1 < FUIIC < FUIIC-3. According to this order, all examined structures exhibit a lower λ_h value than reference FUIIC except FUIIC-3. The tailored molecules FUIIC-2 revealed the lowest λ_h value than all other structures, possibly due to the additional two terminal groups. Overall, FUIIC-2 has minimum values of λ_e and λ_h , which is why it offers a maximum hole and electron transfer rate so that it would be a good structure for use in solar cell devices. The preceding discussion makes it evident that all designed molecules can act as excellent electron- and hole-transfer candidates with better potential reorganizational energy features than reference.

2.5. Open-Circuit Voltage. The V_{oc} can also be used to assess the function of OSCs. The V_{oc} can be defined as the highest quantity of voltage that can be obtained via any display device. It is the maximum voltage at the zero current stage, and this information was obtained via solar technology.⁴⁴ Mainly, two types of current affect the V_{oc} values, one is saturation voltage and the other is photo-generated current. Equation 1 is used to find V_{oc} values of FUIIC and FUIIC-1–FUIIC-6.

$$V_{oc} = (|E_{HOMO}^D| - |E_{LUMO}^A|) - 0.3 \quad (1)$$

A larger V_{oc} is a result of a faster rate of electron transport from the donor HOMO to the acceptor LUMO. PTBT-T is the most commonly used donor material in the literature. In this work, we took PTBT-T as a donor polymer. The results acquired from eq 1 conducted concerning $HOMO_{PTBT-T} - LUMO_{acceptor} E_g$ are shown in Figure 6.

The V_{oc} for FUIIC and FUIIC-1–FUIIC-6 is computed as: 1.65, 1.52, 1.14, 1.56, 1.39, 1.58, and 1.10 V, respectively. The V_{oc} values for investigated systems are in the following order: FUIIC > FUIIC-5 > FUIIC-3 > FUIIC-1 > FUIIC-4 > FUIIC-2 > FUIIC-6. The newly designed molecules FUIIC-5 and FUIIC-3 exhibit V_{oc} values that are almost equal to reference FUIIC. While other molecules revealed V_{oc} value lower than reference FUIIC. Higher V_{oc} values represent the larger voltage obtained

from the solar cell, high conversion efficiency, and vice versa. All developed molecules of the studied family with sufficient V_{oc} values can be considered better entrants for achieving maximum voltage from the solar cell and high conversion efficiency than the reference.

2.6. TDM Analysis and Exciton Binding Energy (E_b).

TDM is another valuable technique to estimate the transition between the donor and acceptor parts in the excited state.⁴⁵ The hydrogen (H) atoms play no role in transition; basically, they are ignored. TDM analysis for reference FUIIC and designed molecules (FUIIC-1–FUIIC-6) were computed with S1 state under vacuum at MPW1PW91/6-31G(d,p) level of theory. In the current investigation, the designed molecules are divided into two parts: core (D) and acceptor. TDM results for all molecules, including reference, are shown in Figure 7. In FUIIC and designed FUIIC-1–FUIIC-6 molecules, almost similar segment contributed in CT, as indicated with heat maps. Transfer of charge occurred from atom number 1–21 designated as D in the TDM surfaces of all investigated molecules. Charge is found to be shifted in the acceptor segment with atom numbers 31–61 in all studied molecules.

TDM pictures depicted that all investigated structures exhibit consistency of charges. A diagonal electron coherence transfer is envisioned for all investigated molecules FUIIC-1–FUIIC-6 and reference FUIIC. The presence of electron coherence in investigated molecules FUIIC and FUIIC-1–FUIIC-6 assures that charge consistency effectively transfers from the central donor part to the bridging unit, facilitating the shifting of electrons without tapping them. Finally, the charge density shifts to another end-capped unit. Figure 7 represents the TDM functionality and charge distribution, which is very important for developing the solar cell.

Binding energy is also significant for evaluating the OSC efficiency. Smaller E_b values boost exciton dissociation by reducing hole–electron Coulombic forces.⁴⁶ Small Coulombic communication among hole and electron facilitates the separation of charge.⁴⁷ The binding energy is equal to the difference between the initial excitation energy E_{opt} and the energy gap (E_g) calculated utilizing eq 2, and the results are given in Table 5.

$$E_b = E_{H-L} - E_{opt} \quad (2)$$

The E_b energy of FUIIC is computed as 0.40 eV. The E_b of FUIIC-1–FUIIC-6 is noted as 0.45, 0.43, 0.47, 0.44, 0.44, and 0.44 eV, correspondingly. The declining sequence of E_b for all structures, including reference, is FUIIC < FUIIC-2 < FUIIC-4 = FUIIC-5 = FUIIC-6 < FUIIC-1 < FUIIC-3. These calculated values indicate that FUIIC-4, FUIIC-5, and FUIIC-6 have E_b values that are almost similar to those of the FUIIC molecule. It

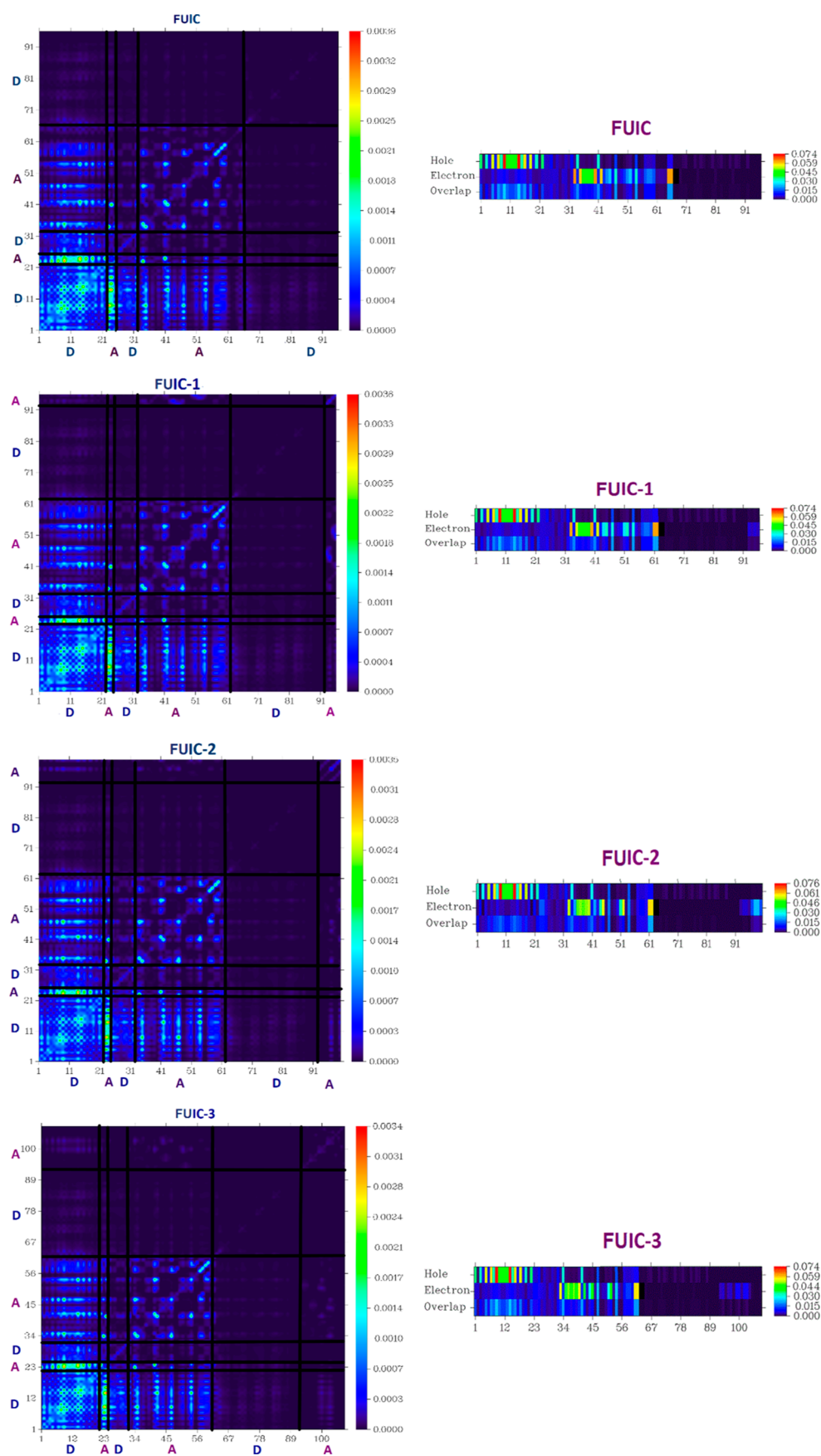


Figure 7. continued

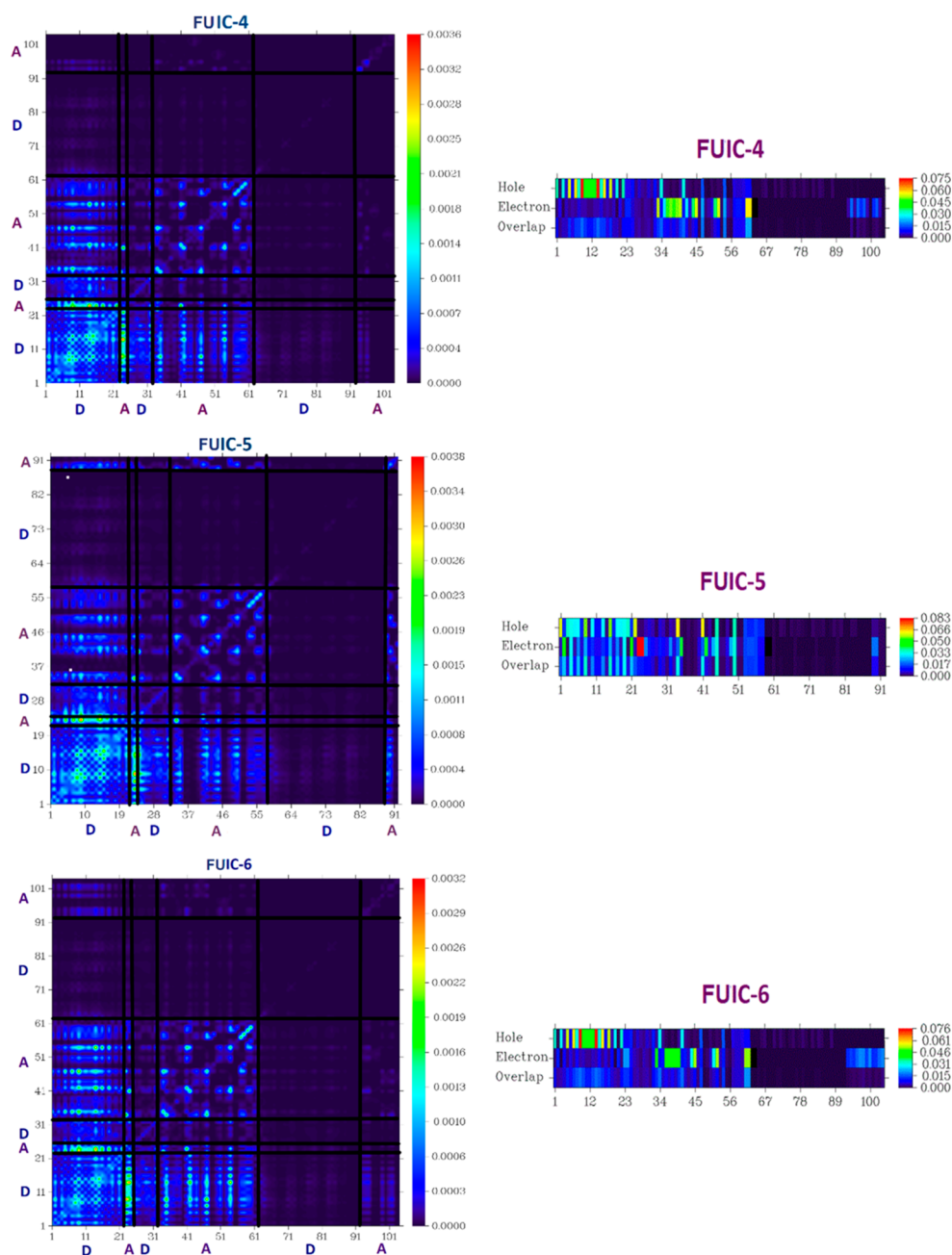


Figure 7. TDM surfaces for all reference and designed molecules.

Table 5. Exciton Binding Energies (E_b) of FUIC and FUIC-1–FUIC-6

molecules	E_{H-L} (eV)	E_{opt} (eV)	E_b (eV)
FUIC	2.00	1.60	0.40
FUIC-1	2.01	1.56	0.45
FUIC-2	1.90	1.47	0.43
FUIC-3	2.01	1.54	0.47
FUIC-4	1.96	1.52	0.44
FUIC-5	2.01	1.57	0.44
FUIC-6	1.88	1.44	0.44

may be due to additional end-capped groups. As a result, these constructed compounds can be used as good acceptor molecules in OSCs.

2.7. Charge-Transfer Analysis between PBDT-T and FUIC-6. In order to verify that the created molecules may be used in solar cell materials, CT analysis is performed on them. For this, the acceptor molecules are modeled into a layer that contains a well-known and well-characterized donor. Among the investigated systems, the FUIC-6 molecule was chosen for charge-transfer analysis with an established PBDT-T polymer, and the PBDT-T/FUIC-6 complex has been optimized. This was due to the FUIC-6 molecule having the lowest energy gap, the lowest E_x , the lowest E_b , the lowest λ_h and λ_e values, and the highest λ_{max} values. Figure 8 depicts the PBDT-T/FUIC-6 complex optimized shape at the MPW1PW91/6-31G(d,p) functional.

Figure 8 depicts the relative positions of PBDT-T and FUIC-6. The orientation of the PBDT-T/FUIC-6 complex is also helpful for the electron-transfer process. To facilitate

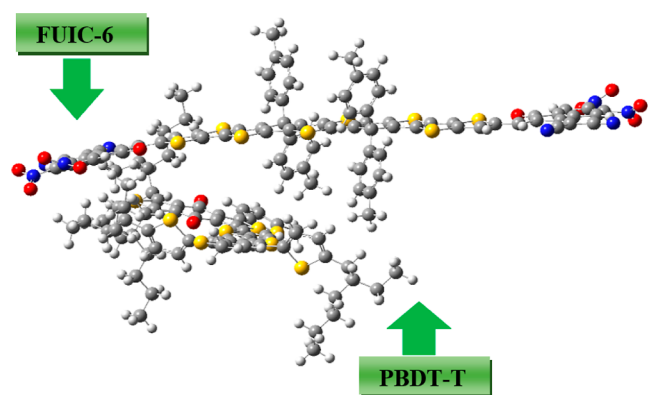


Figure 8. Optimized structure of the PBDT-T and FUIC-6 complex.

electron transport between donor and acceptor moieties, the core regions of FUIC-6 and PBDT-T are arranged in a parallel fashion. The aforesaid complex was then used to get the HOMO and LUMO. The HOMO charge is localized on the donor polymer, while the LUMO charge is dispersed across the FUIC-6 acceptor molecule. There is promising evidence that tailored molecules can be useful in real-world solar cell applications, thanks to the transmission of charge density from the donor (HOMO) to the acceptor (LUMO) layer in the PBDT-T/FUIC-6 blend (Figure 9).

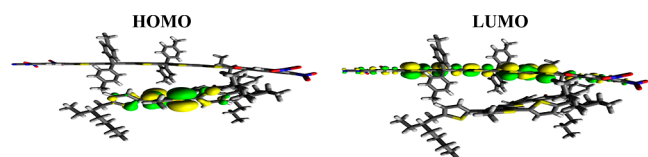


Figure 9. HOMO and LUMO calculated from the PBDT-T and FUIC-6 complex.

In silico engineering of thieno[2,3-*b*]thiophene core-based non-fullerene acceptors will lead to new developments in the next years, such as non-fullerene electron acceptors with larger solar spectrum absorption and fine optoelectronic characteristics. It raises hopes for high OSC PCE in the coming years.

3. CONCLUSIONS

In conclusion, advanced quantum chemical methods have been utilized to investigate the behavior of CT, structure–activity, photovoltaic and optoelectronic characteristics of six novel fused-ring, highly conjugated A– π –D– π –A designed structures FUIC-1–FUIC-6 designed by substituting the end-capped acceptors and compared with FUIC molecules. The UV–visible graphs showed that maximum absorption values of designed molecules shifted toward longer wavelengths in the range of 780.01–862.31 nm in the solvent phase while 728.24–776.98 nm in the gas phase in comparison to the reference molecule having 780.01 nm in the solvent and 717.71 nm in the gas phase. The HOMO–LUMO energy gap values of FUIC-1–FUIC-6 are reduced to 2.01–1.88 eV by end-capped acceptor substitution compared with FUIC 1.99 eV. The binding energy of the constructed structures is comparable to the reference FUIC, resulting in increased exciton dissociation in the excited state. The values of reorganizational energies of electron and hole of FUIC-1–FUIC-6 are observed to be lower than FUIC in the molecule. Consequently, the ascending sequence of open-circuit voltage

is FUIC > FUIC-5 > FUIC-3 > FUIC-1 > FUIC-4 > FUIC-2 > FUIC-6 and found to be in better accordance with the ascending order of the excitation energy as follows FUIC-6 < FUIC-2 < FUIC-4 < FUIC-3 < FUIC-1 < FUIC-5 < FUIC. The increasing sequence of maximum absorption values is FUIC-6 > FUIC-2 > FUIC-4 > FUIC-3 > FUIC-1 > FUIC-5 > FUIC both in the solvent and gas phase. According to all analyses, FUIC-6 is the best and most efficient molecule among all investigated compounds because of its electron-withdrawing capacity and prolonged conjugation of the terminal acceptors (end-capped) of FUIC-6 due to the presence of NO₂ groups. It possesses excellent photovoltaic features like less band gap (1.88 eV), lowest $\lambda_e = 0.00431856$ eV and $\lambda_h = 0.00806781$ eV, largest λ_{max} values 862.31 nm (in solvent) and 776.98 nm (in gas), and $V_{oc} = 1.1$ V concerning HOMO_{PBDT-T}–LUMO_{acceptor}. Our findings indicate that the designed structures, especially FUIC-6, are efficient acceptor moieties employed as hole- and electron-transporting material in OSCs with outstanding photovoltaic characteristics and can be used in future high-performance OSC systems.

4. COMPUTATIONAL PROCEDURES

The Gaussian 09 program was utilized to conduct all quantum chemistry studies.⁴⁸ Using GaussView 5.0,⁴⁹ all input files of reference and designed molecules (FUIC and FUIC-1–FUIC-6) are prepared. First, reference molecule is optimized using density DFT calculations at six different functionals, including B3LYP,⁵⁰ CAM-B3LYP,⁵¹ M06-2X,⁵² MPW1PW91,⁵³ and ω B97XD⁵⁴ in combination with 6-31G(d,p) basis set. After frequency calculations of reference FUIC, the λ_{max} (maximum absorption) was calculated. The λ_{max} values calculated for the FUIC molecule at six different functionals were compared to the λ_{max} values reported experimentally.²⁴ The MPW1PW91/6-31G(d,p) functional was selected as the best functional among all six due to good harmony with the experimental value. The opted functional delivered strong evidence to undertake further all calculations of FUIC and constructed molecules (FUIC-1–FUIC-6). Therefore, optimizing designed molecules (FUIC-1–FUIC-6) was executed using selected functional. A vibrational study at the same opted functional was carried out to confirm the absence of negative eigenvalues and the appearance of optimized geometries in the lowest potential energy surfaces. The absorption spectrum of investigated molecules FUIC and FUIC-1–FUIC-6 was estimated by means of the CPCM model⁵⁵ in the chloroform solvent at MPW1PW91/6-31G(d,p) functional. For the determination of λ_{max} (in the solvent and gas), Swizard software was applied. Using Origin 8.0 software, the results of Gaussian calculations were shown. DFT/MPW1PW91/6-31G(d,p) functional was applied to measure different parameters, including FMOs, DOS calculations, reorganizational energies, TDM analysis, V_{oc} analysis of CT, and energy band gap of (FUIC and FUIC-1–FUIC-6) molecules. The DOS for all investigated molecules was calculated and displayed using PyMolyze 2.0⁵⁶ software to determine the percentage impact of acceptor and donor fragments for radiation absorption. Electronic excitation transition density matrix (TDM) analysis is executed using Multiwfn 3.7 software.⁵⁷ There are two different kinds of reorganization energies. Internal reorganization (λ_{int}) is first and is concerned with the internal structures of molecules, while the second is referred to as external reorganization (λ_{ext}) and is concerned with the external environment, and its effect was ignored in

this report because it is not very effective.⁵⁸ For the CT study of all molecules, whether intermolecular or intramolecular, Marcus theory⁵⁹ is very important. The following eq 3 can be used to understand electron mobility (λ_e) in terms of Marcus theory.

$$\lambda_e = [E_0^- - E_-] + [E_-^0 - E_0] \quad (3)$$

Furthermore, hole mobility (λ_h) is also essential for CT interactions in OSCs. Its value can be calculated using the formula given below

$$\lambda_h = [E_0^+ - E_+] + [E_+^0 - E_0] \quad (4)$$

In these eqs 3, 4, the anion and cation single-point energies E_0^- and E_0^+ are found by optimizing neutral molecules. By their respective optimal geometries, cation and anion energies are denoted by E_- and E_+ . The energies of the neutral molecule are represented by E_-^0 and E_+^0 , which are obtained by optimizing the cation and anion energies, respectively. The energy of a neutral molecule in its ground state is denoted by the symbol E_0 .⁶⁰

AUTHOR INFORMATION

Corresponding Authors

Saleh S. Alarfaji – Department of Chemistry, Faculty of Science, King Khalid University, Abha 61413, Saudi Arabia; Research Center for Advanced Materials Science (RCAMS), King Khalid University, Abha 61514, Saudi Arabia; orcid.org/0000-0001-7297-7185; Email: ssalarvagi@kku.edu.sa

Riaz Hussain – Department of Chemistry, Division of Science and Technology, University of Education Lahore, Dera Ghazi Khan 54000, Pakistan; orcid.org/0000-0002-6154-1244; Email: riaz.hussain@ue.edu.pkk

Authors

Faiz Rasool – Institute of Chemical Sciences Bahauddin Zakariya University, Multan 60800, Pakistan

Bushra Iqbal – Institute of Chemistry, Khwaja Fareed University of Engineering & Information Technology, Rahim Yar Khan 64200, Pakistan

Ajaz Hussain – Institute of Chemical Sciences Bahauddin Zakariya University, Multan 60800, Pakistan

Muhammad Akhlaq – Faculty of Pharmacy, Gomal University, Dera Ismail Khan 29050, Pakistan

Muhammad Fayyaz ur Rehman – Department of Chemistry, University of Sargodha, Sargodha 40100, Pakistan; orcid.org/0000-0003-2901-7212

Complete contact information is available at: <https://pubs.acs.org/10.1021/acsomega.2c06877>

Notes

The authors declare no competing financial interest.

ACKNOWLEDGMENTS

S.S.A. extends his appreciation to the Deanship of Scientific Research at King Khalid University for funding this work through Large Group Research Project under grant number 34/43, and S.S.A. also acknowledges the Research Center for Advance Materials (RCAMS) at King Khalid University, Saudi Arabia for their valuable technical support.

REFERENCES

- (1) Chaudhary, S.; Mehra, R. *Advances in Solar Cells as Renewable Energy. Proceedings of International Conference on Advancements in Computing & Management (ICACM) 2019*; SSRN, 2019.
- (2) Hosenuzzaman, M.; Rahim, N. A.; Selvaraj, J.; Hasanuzzaman, M.; Malek, A. A.; Nahar, A. Global prospects, progress, policies, and environmental impact of solar photovoltaic power generation. *Renew. Sustain. Energy Rev.* **2015**, *41*, 284–297.
- (3) Khalid, M.; Shafiq, I.; Zhu, M.; Khan, M. U.; Shafiq, Z.; Iqbal, J.; Alam, M. M.; Braga, A. A. C.; Imran, M. Efficient tuning of small acceptor chromophores with A1- π -A2- π -A1 configuration for high efficacy of organic solar cells via end group manipulation. *J. Saudi Chem. Soc.* **2021**, *25*, 101305.
- (4) Khan, M. U.; Iqbal, J.; Khalid, M.; Hussain, R.; Braga, A. A. C.; Hussain, M.; Muhammad, S. Designing triazatruxene-based donor materials with promising photovoltaic parameters for organic solar cells. *RSC Adv.* **2019**, *9*, 26402–26418.
- (5) Khalid, M.; Momina; Imran, M.; Rehman, M. F. u.; Braga, A. A. C.; Akram, M. S. Molecular engineering of indenodene-3-ethylrodanine acceptors with A2-A1-D-A1-A2 architecture for promising fullerene-free organic solar cells. *Sci. Rep.* **2021**, *11*, 20320.
- (6) Lu, L.; Zheng, T.; Wu, Q.; Schneider, A. M.; Zhao, D.; Yu, L. Recent Advances in Bulk Heterojunction Polymer Solar Cells. *Chem. Rev.* **2015**, *115*, 12666–12731.
- (7) Armin, A.; Li, W.; Sandberg, O. J.; Xiao, Z.; Ding, L.; Nelson, J.; Neher, D.; Vandewal, K.; Shoaee, S.; Wang, T.; Ade, H.; Heumüller, T.; Brabec, C.; Meredith, P. A History and Perspective of Non-Fullerene Electron Acceptors for Organic Solar Cells. *Adv. Energy Mater.* **2021**, *11*, 2003570.
- (8) Riede, M.; Spoltore, D.; Leo, K. Organic Solar Cells-The Path to Commercial Success. *Adv. Energy Mater.* **2021**, *11*, 2002653.
- (9) Cao, D. H.; Stoumpos, C. C.; Farha, O. K.; Hupp, J. T.; Kanatzidis, M. G. 2D homologous perovskites as light-absorbing materials for solar cell applications. *J. Am. Chem. Soc.* **2015**, *137*, 7843–7850.
- (10) Xu, C.; Ma, X.; Zhao, Z.; Jiang, M.; Hu, Z.; Gao, J.; Deng, Z.; Zhou, Z.; An, Q.; Zhang, J.; Zhang, F. Over 17.6% efficiency organic photovoltaic devices with two compatible polymer donors. *Sol. RRL* **2021**, *5*, 2100175.
- (11) Xu, C.; Jin, K.; Xiao, Z.; Zhao, Z.; Yan, Y.; Zhu, X.; Li, X.; Zhou, Z.; Jeong, S. Y.; Ding, L.; Woo, H. Y.; Yuan, G.; Zhang, F. Efficient Semitransparent Layer-by-Layer Organic Photovoltaics via Optimizing Wide Bandgap and Narrow Absorption Polymer Layer Thickness. *Sol. RRL* **2022**, *6*, 2200308.
- (12) Xu, W.; Zhu, X.; Ma, X.; Zhou, H.; Li, X.; Jeong, S. Y.; Woo, H. Y.; Zhou, Z.; Sun, Q.; Zhang, F. Achieving 15.81% and 15.29% efficiency of all-polymer solar cells based on layer-by-layer or bulk heterojunction structure. *J. Mater. Chem. A* **2022**, *10*, 13492.
- (13) Ma, X.; Jiang, Q.; Xu, W.; Xu, C.; Jeong, S. Y.; Woo, H. Y.; Wu, Q.; Zhang, X.; Yuan, G.; Zhang, F. Layered optimization strategy enables over 17.8% efficiency of layer-by-layer organic photovoltaics. *Chem. Eng. J.* **2022**, *442*, 136368.
- (14) Zhang, Y.; Ji, Y.; Zhang, Y.; Zhang, W.; Bai, H.; Du, M.; Wu, H.; Guo, Q.; Zhou, E. Recent Progress of Y6-Derived Asymmetric Fused Ring Electron Acceptors. *Adv. Funct. Mater.* **2022**, *32*, 2205115.
- (15) Nie, Q.; Tang, A.; Guo, Q.; Zhou, E. Benzothiadiazole-based non-fullerene acceptors. *Nano Energy* **2021**, *87*, 106174.
- (16) Yang, J.; Xiao, B.; Tang, A.; Li, J.; Wang, X.; Zhou, E. Aromatic-Diimide-Based n-Type Conjugated Polymers for All-Polymer Solar Cell Applications. *Adv. Mater.* **2019**, *31*, 1804699.
- (17) Lin, Y.; Wang, J.; Zhang, Z. G.; Bai, H.; Li, Y.; Zhu, D.; Zhan, X. An electron acceptor challenging fullerenes for efficient polymer solar cells. *Adv. Mater.* **2015**, *27*, 1170–1174.
- (18) Dai, S.; Xiao, Y.; Xue, P.; James Rech, J.; Liu, K.; Li, Z.; Lu, X.; You, W.; Zhan, X. Effect of core size on performance of fused-ring electron acceptors. *Chem. Mater.* **2018**, *30*, 5390–5396.
- (19) Li, T.; Dai, S.; Ke, Z.; Yang, L.; Wang, J.; Yan, C.; Ma, W.; Zhan, X. Fused Tris(thienothiophene)-Based Electron Acceptor with

Strong Near-Infrared Absorption for High-Performance As-Cast Solar Cells. *Adv. Mater.* **2018**, *30*, 1705969.

(20) Katan, C.; Tretiak, S.; Werts, M. H.; Bain, A. J.; Marsh, R. J.; Leonczek, N.; Nicolaou, N.; Badaeva, E.; Mongin, O.; Blanchard-Desce, M. Two-photon transitions in quadrupolar and branched chromophores: experiment and theory. *J. Phys. Chem. B* **2007**, *111*, 9468–9483.

(21) Delgado, M. C. R.; Kim, E.-G.; Filho, D. t. A. d. S.; Bredas, J.-L. Tuning the charge-transport parameters of perylene diimide single crystals via end and/or core functionalization: a density functional theory investigation. *J. Am. Chem. Soc.* **2010**, *132*, 3375–3387.

(22) Terenziani, F.; Katan, C.; Badaeva, E.; Tretiak, S.; Blanchard-Desce, M. Enhanced Two-Photon Absorption of Organic Chromophores: Theoretical and Experimental Assessments. *Adv. Mater.* **2008**, *20*, 4641–4678.

(23) Pawlicki, M.; Collins, H. A.; Denning, R. G.; Anderson, H. L. Two-Photon Absorption and the Design of Two-Photon Dyes. *Angew. Chem., Int. Ed.* **2009**, *48*, 3244–3266.

(24) Allen, T. G.; Benis, S.; Munera, N.; Zhang, J.; Dai, S.; Li, T.; Jia, B.; Wang, W.; Barlow, S.; Hagan, D. J.; Van Stryland, E. W.; Zhan, X.; Perry, J. W.; Marder, S. R. Highly Conjugated, Fused-Ring, Quadrupolar Organic Chromophores with Large Two-Photon Absorption Cross-Sections in the Near-Infrared. *J. Phys. Chem. A* **2020**, *124*, 4367–4378.

(25) Liu, Y.; Page, Z. A.; Russell, T. P.; Emrick, T. Finely tuned polymer interlayers enhance solar cell efficiency. *Angew. Chem.* **2015**, *127*, 11647–11651.

(26) Spanggaard, H.; Krebs, F. C. A brief history of the development of organic and polymeric photovoltaics. *Sol. Energy Mater. Sol. Cells* **2004**, *83*, 125–146.

(27) Biswas, S.; Pramanik, A.; Sarkar, P. Effect of additional donor group on the charge transfer/recombination dynamics of a photoactive organic dye: A quantum mechanical investigation. *Comput. Theor. Chem.* **2017**, *1103*, 38–47.

(28) Biswas, S.; Pramanik, A.; Sarkar, P. Origin of different photovoltaic activities in regioisomeric small organic molecule solar cells: the intrinsic role of charge transfer processes. *J. Phys. Chem. C* **2018**, *122*, 14296–14303.

(29) Raheem, A. A.; Kamaraj, S.; Sannasi, V.; Praveen, C. New D- π -A push-pull chromophores as low band gap molecular semiconductors for organic small molecule solar cell applications. *Org. Chem. Front.* **2018**, *5*, 777–787.

(30) Ma, W.; Jiao, Y.; Meng, S. Modeling charge recombination in dye-sensitized solar cells using first-principles electron dynamics: effects of structural modification. *Phys. Chem. Chem. Phys.* **2013**, *15*, 17187–17194.

(31) Imran, M.; Khalid, M.; Jawaria, R.; Ali, A.; Asghar, M. A.; Shafiq, Z.; Assiri, M. A.; Lodhi, H. M.; Braga, A. A. C. Exploration of Photophysical and Nonlinear Properties of Salicylaldehyde-Based Functionalized Materials: A Facile Synthetic and DFT Approach. *ACS Omega* **2021**, *6*, 33914–33922.

(32) Khalid, M.; Khan, M. U.; Hussain, R.; Irshad, S.; Ali, B.; Braga, A. A. C.; Imran, M.; Hussain, A. Exploration of second and third order nonlinear optical properties for theoretical framework of organic D- π -D- π -A type compounds. *Opt. Quant. Electron.* **2021**, *53*, 561.

(33) Khalid, M.; Khan, M. U.; Razia, E.-t.; Shafiq, Z.; Alam, M. M.; Imran, M.; Akram, M. S. Exploration of efficient electron acceptors for organic solar cells: rational design of indacenodithiophene based non-fullerene compounds. *Sci. Rep.* **2021**, *11*, 19931.

(34) Ashfaq, M.; Ali, A.; Nawaz Tahir, M. N.; Khalid, M.; Assiri, M. A.; Imran, M.; Shahzad Munawar, K. S.; Habiba, U. Synthetic approach to achieve halo imine units: Solid-state assembly, DFT based electronic and non linear optical behavior. *Chem. Phys. Lett.* **2022**, *803*, 139843.

(35) Mahmood, A.; Abdullah, M. I.; Nazar, M. F. Quantum chemical designing of novel organic non-linear optical compounds. *Bull. Korean Chem. Soc.* **2014**, *35*, 1391–1396.

(36) Khalid, M.; Zafar, M.; Hussain, S.; Asghar, M. A.; Khera, R. A.; Imran, M.; Abookleesh, F. L.; Akram, M. Y.; Ullah, A. Influence of

End-Capped Modifications in the Nonlinear Optical Amplitude of Nonfullerene-Based Chromophores with a D- π -A Architecture: A DFT/TDDFT Study. *ACS Omega* **2022**, *7*, 23532–23548.

(37) Hassan, T.; Hussain, R.; Khan, M. U.; Habiba, U.; Irshad, Z.; Adnan, M.; Lim, J. Development of non-fused acceptor materials with 3D-Interpenetrated structure for stable and efficient organic solar cells. *Mater. Sci. Semicond. Process.* **2022**, *151*, 107010.

(38) Rafiq, A.; Hussain, R.; Khan, M. U.; Mehboob, M. Y.; Khalid, M.; Shehnaz, M. M.; Alam, M.; Imran, K.; Ayub, K. Novel Star-Shaped Benzotriindole-Based Nonfullerene Donor Materials: Toward the Development of Promising Photovoltaic Compounds for High-Performance Organic Solar Cells. *Energy Technol.* **2022**, *10*, 2100751.

(39) Mahmood, A.; Khan, S. U.-D.; Rana, U. A.; Tahir, M. H. Red shifting of absorption maxima of phenothiazine based dyes by incorporating electron-deficient thiadiazole derivatives as π -spacer. *Arab. J. Chem.* **2019**, *12*, 1447–1453.

(40) Mahmood, A.; Hussain Tahir, M.; Irfan, A.; Khalid, B.; Al-Sehemi, A. G. Computational Designing of Triphenylamine Dyes with Broad and Red-shifted Absorption Spectra for Dye-sensitized Solar Cells using Multi-Thiophene Rings in π -Spacer. *Bull. Korean Chem. Soc.* **2015**, *36*, 2615–2620.

(41) Mahmood, A.; Irfan, A. Computational analysis to understand the performance difference between two small-molecule acceptors differing in their terminal electron-deficient group. *J. Comput. Electron.* **2020**, *19*, 931–939.

(42) Khalid, M.; Khan, M. U.; Ahmed, S.; Shafiq, Z.; Alam, M. M.; Imran, M.; Braga, A. A. C.; Akram, M. S. Exploration of promising optical and electronic properties of (non-polymer) small donor molecules for organic solar cells. *Sci. Rep.* **2021**, *11*, 21540.

(43) Khan, M. U.; Khalid, M.; Hussain, R.; Umar, A.; Mehboob, M. Y.; Shafiq, Z.; Imran, M.; Irfan, A. Novel W-Shaped Oxygen Heterocycle-Fused Fluorene-Based Non-Fullerene Acceptors: First Theoretical Framework for Designing Environment-Friendly Organic Solar Cells. *Energy Fuels* **2021**, *35*, 12436–12450.

(44) Janjua, M. R. S. A.; Khan, M. U.; Khalid, M.; Ullah, N.; Kalgaonkar, R.; Alnoaimi, K.; Baqader, N.; Jamil, S. Theoretical and conceptual framework to design efficient dye-sensitized solar cells (DSSCs): molecular engineering by DFT method. *J. Cluster Sci.* **2021**, *32*, 243–253.

(45) Khan, M. U.; Khalid, M.; Arshad, M. N.; Khan, M. N.; Usman, M.; Ali, A.; Saifullah, B. Designing Star-Shaped Subphthalocyanine-Based Acceptor Materials with Promising Photovoltaic Parameters for Non-fullerene Solar Cells. *ACS Omega* **2020**, *5*, 23039–23052.

(46) Mahmood, A.; Irfan, A. Effect of fluorination on exciton binding energy and electronic coupling in small molecule acceptors for organic solar cells. *Comput. Theor. Chem.* **2020**, *1179*, 112797.

(47) Mahmood, A.; Khan, S. U.-D.; Rana, U. A. Theoretical designing of novel heterocyclic azo dyes for dye sensitized solar cells. *J. Comput. Electron.* **2014**, *13*, 1033–1041.

(48) Frisch, M. J.; Trucks, G. W.; Schlegel, H. B.; Scuseria, G.; Robb, M. A.; Cheeseman, J. R.; Scalmani, G.; Barone, V.; Mennucci, B.; Petersson, G.; et al. *Gaussian 09*, Revision D. 01; Gaussian, Inc.: Wallingford, CT, 2009.

(49) Dennington, R. D.; Keith, T. A.; Millam, J. M. *GaussView 5.0*. 8; Gaussian Inc., 2008.

(50) Civalieri, B.; Zicovich-Wilson, C. M.; Valenzano, L.; Ugliengo, P. B3LYP augmented with an empirical dispersion term (B3LYP-D*) as applied to molecular crystals. *CrystEngComm* **2008**, *10*, 405–410.

(51) Yanai, T.; Tew, D. P.; Handy, N. C. A new hybrid exchange-correlation functional using the Coulomb-attenuating method (CAM-B3LYP). *Chem. Phys. Lett.* **2004**, *393*, 51–57.

(52) Zhao, Y.; Truhlar, D. G. The M06 suite of density functionals for main group thermochemistry, thermochemical kinetics, non-covalent interactions, excited states, and transition elements: two new functionals and systematic testing of four M06-class functionals and 12 other functionals. *Theor. Chem. Acc.* **2008**, *120*, 215–241.

(53) Adamo, C.; Barone, V. Exchange functionals with improved long-range behavior and adiabatic connection methods without

adjustable parameters: The mPW and mPW1PW models. *J. Chem. Phys.* **1998**, *108*, 664–675.

(54) Chai, J.-D.; Head-Gordon, M. Long-range corrected hybrid density functionals with damped atom-atom dispersion corrections. *Phys. Chem. Chem. Phys.* **2008**, *10*, 6615–6620.

(55) Barone, V.; Cossi, M. Quantum calculation of molecular energies and energy gradients in solution by a conductor solvent model. *J. Phys. Chem. A* **1998**, *102*, 1995–2001.

(56) O'boyle, N. M.; Tenderholt, A. L.; Langner, K. M. cclib: A library for package-independent computational chemistry algorithms. *J. Comput. Chem.* **2008**, *29*, 839–845.

(57) Lu, T.; Chen, F. Multiwfn: a multifunctional wavefunction analyzer. *J. Comput. Chem.* **2012**, *33*, 580–592.

(58) Ans, M.; Ayub, K.; Bhatti, I. A.; Iqbal, J. Designing indacenodithiophene based non-fullerene acceptors with a donor-acceptor combined bridge for organic solar cells. *RSC Adv.* **2019**, *9*, 3605–3617.

(59) Marcus, R. A. Electron transfer reactions in chemistry. Theory and experiment. *Rev. Mod. Phys.* **1993**, *65*, 599.

(60) Tang, S.; Zhang, J. Design of donors with broad absorption regions and suitable frontier molecular orbitals to match typical acceptors via substitution on oligo(thienylenevinylene) toward solar cells. *J. Comput. Chem.* **2012**, *33*, 1353–1363.